Uniform needle-emitter arrays for ionic liquid electrospray thrusters with precise thrust control

Fumiya Tachibana[1], Toshiyuki Tsuchiya[2], and Yoshinori Takao[3*]

[1]*Department of Mechanical Engineering, Materials Science, and Ocean Engineering, Yokohama National University, 79-5 Tokiwadai, Hodogaya-ku, Yokohama, Kanagawa 240-8501, Japan*

[2]*Department of Micro Engineering, Kyoto University, C3 Bldg., Kyoto University-Katsura, Nishikyo-ku, Kyoto 615-8540, Japan*

[3]*Division of Systems Research, Yokohama National University, 79-5 Tokiwadai, Hodogaya-ku, Yokohama, Kanagawa 240-8501, Japan*

*E-mail: takao@ynu.ac.jp

Abstract

The development of ionic liquid electrospray thrusters with highly precise needle-emitter arrays is reported. Micro-electro-mechanical systems process technology is applied in the fabrication process of needle-emitter arrays to achieve a uniform shape of emitter tips. The resulting emitter-array chips were then tested to gather the current–voltage characteristics of emitter

arrays with different numbers of emitters. The maximum ion current extracted from the emitters increased almost in proportion with the number of emitters. When the current–voltage curves of 81-, 169-, and 361-emitter chips were compared with a constant gap distance between the emitter and extractor electrodes, the onset voltage of ion emission was nearly constant because the emitter tips on all the chips were uniform in shape. Moreover, the current–voltage curves had similar slopes for the different number of emitters after the onset voltage, which demonstrates the uniform ion current output of all the emitter arrays.

1. Introduction

The number of launched nano/microsatellites has been increasing since 2013; more than 300 nano/microsatellites were launched in 2017.[1)] Because nano/microsatellites can be developed quickly and at a low cost,[2)] small companies and universities as well as large companies and government agencies can make and operate nano/microsatellites.[3–10)] These satellites (< 100 kg) are now deployed for diverse applications, and advanced missions, such as formation flights and constellations of nano/microsatellites, are now being planned and carried out.[11–13)] Such nano/microsatellite based missions require propulsion systems that can be mounted on nano/microsatellites and achieve precise thrust control to maintain the relative positions of a satellite formation.[14–16)]

Ionic liquid electrospray thrusters hold great potential as miniature propulsion systems with precise thrust control for nano/microsatellites because they neither require a gas propellant nor a neutralizer, which drastically reduces the size of the entire propulsion system compared to conventional alternatives. Figure 1 shows a schematic of a general electrospray thruster. The electrospray thruster comprises needle-shaped emitters and an extractor electrode. By applying a high voltage of about a few kilovolts between the emitters and the extractor electrode, the ionic liquid, which is the propellant of the thruster, flows to the emitters' tips. Because the curvature radius of the emitter tips is only a few micrometers, a strong electric field is generated at the emitter tip. This strong electric field deforms the ionic liquid into a conical structure known as a Taylor cone.[17)] When the force of the electric field is stronger than the surface

tension pressure of the ionic liquid, ions evaporate directly from the surface. The extracted ions are then accelerated by the potential difference between the emitters and the extractor electrode to produce thrust.[18,19)]

Ionic liquids are molten salts that consist of only positive and negative ions (cations and anions), and their vapor pressure is nearly zero because of the strong Coulomb forces between the ions.[20)] Coulomb interactions allow ionic liquids to remain in the liquid phase even in vacuum, making it easier to store the propellant in a compact package as compared with electric propulsion systems that use gas propellants, e.g., ion thrusters. In addition, high-pressure gas feed systems, which require mechanical valves for gas flow control can be eliminated in electrospray thrusters, thus eliminating mechanical vibrations from the system and further enhancing the precision of thrust control. Moreover, electrospray thrusters can extract cations and anions by applying a positive or negative voltage to the emitters, respectively. This feature eliminates the need for neutralizers as cations and anions can be extracted alternately with bipolar pulse voltage, or both the ions can be extracted simultaneously using a pair of electrospray thrusters.[21,22)] Although neutralizers cannot yield thrust owing to the very small mass of electrons, anions can generate thrust because anions and cations have similar molecular weights. Furthermore, because each emitter of an electrospray thruster produces only a small amount of thrust (of the order of 10 nN), the thrust can be controlled precisely by adjusting the number of emitters and the voltage applied to the emitters.

In our previous study, we fabricated externally-wetted needle-shaped emitters by using

micro-electro-mechanical systems (MEMS) processing and we conducted ion current measurements to develop ionic liquid electrospray thrusters.[23] The resulting maximum extracted ion current with four emitters was about 8 μA at an applied voltage of 3700 V, and the thrust was estimated to be 0.77 μN. However, the extracted ion current hardly increased with increase in the number of emitters because the emitter tips were nonuniform.

This lack of uniformity meant that the number of emitters in an array could not be used to control the ion current. The present study addresses this issue with the fabrication of a uniform emitter array and conduction of ion emission experiments that use the emitter arrays in electrospray thrusters. Here, we report a MEMS process that yields arrays with uniform emitter tips and the current–voltage characteristics of emitter chips with different numbers of emitters.

The rest of the paper is organized as follows. In Sect. 2, we describe the fabrication process and the ion emission experiment of emitter chips with one and nine emitters. Because the ion current did not increase with the number of emitters in tests with these small chips, the fabrication process was revised to achieve better uniformity in the emitter tips. This revised process and test results with 81-, 169-, and 361-emitter chips are then discussed in Sect. 3. Section 4 draws conclusions to this study.

2. Fabrication and current measurements of single and nine-emitter arrays

First, we fabricated emitter chips with one and nine emitters to compare the ion current

output. These preliminary tests with small numbers of emitters were designed to clarify whether the ion current would depend on the number of emitters with the MEMS fabrication process.

2.1. Fabrication process

We fabricated the emitter chips using the steps that are illustrated in Fig. 2. First, we coated a silicon wafer with a thick positive-type photoresist (PMER P-LA900PM). This positive-type photoresist was transcribed from a photomask pattern by using photolithography. Second, we performed isotropic etching using SF_6 to form the cone shape of the emitter tips, based on the patterned photoresist layer. Then, the ionic liquid reservoir was formed by the Bosch process,[24,25] after which the photoresist was removed. Figure 3 shows the fabricated chips with a single emitter and an array of nine emitters. Both emitter chips are 10 mm × 10 mm in dimension, and the central region (8 mm in diameter) forms the ionic liquid reservoir, which encompasses the emitters. For the single emitter, the diameters of the emitter base and tip are 100 μm and 6 μm, respectively. The nine emitters in the array are aligned in a straight line with the pitch of 500 μm, and all the emitter bases are 100 μm in diameter. However, as shown in Figs. 3(e) and 3(f), the emitter-tip diameters came out different; the tip diameter at the center of the array is 12 μm, while the emitter at the left end is only 1 μm in diameter.

These differences in tip diameter were caused by nonuniform isotropic etching.[23] In the isotropic etching process shown in Fig. 2(b), the etching rate increased in proportion to the distance from the center of the emitter array because of local variations in the pattern density and total exposed area.[26] In addition, the etching rate varied with position within a single silicon

wafer. Here, we fabricated four emitter chips on a 4-inch wafer: three emitter chips with a single emitter and one emitter chip with an array of nine emitters, and the etching rate increased in proportion to the distance from the center of the wafer owing to non-uniform plasma density in the process chamber. The non-uniform etching rate, depending on the position within the array and the wafer, was responsible for the nonuniform diameters of the emitter tips.

2.2. Experimental setup

We tested the fabricated emitter chips in ion emission experiments. Figure 4(a) shows a schematic of the experimental setup that we used for ion current measurements. The distance between the emitter tip and extractor was set at d = 0.3 mm, and the collector electrode (18 mm × 30 mm) was placed at a distance of L = 14 mm from the extractor electrode. Most of the systems under test (emitter chip, extractor, and collector) were in a vacuum chamber evacuated by a rotary pump and a turbomolecular pump at a base pressure $<1.0 \times 10^{-3}$ Pa. Figures 4(b) and 4(c) show the extractor electrodes for the single emitter and the array of nine emitters, respectively. The extractor electrodes are 0.08-mm thick metal plates, and contain an aperture that is 0.5 mm in diameter for the single emitter and has 0.5 mm × 5 mm slit for the array of nine emitters. These extractor electrodes were aligned with the emitter chip using the same alignment system employed in our previous paper,[23)] with which alignment must be conducted manually and examined visually. Thus, by merging a row of apertures into a slit, we can easily align the emitter and extractor and reduce the number of ions intercepted by the extractor, although the electric field at the emitter tips will be slightly reduced. We used an ionic liquid

1-ethyl-3-methylimidazolium dicyanamide (EMI-DCA) as a propellant for testing, and placed a small drop of ionic liquid (0.01 μL) on the reservoir to be supplied to the emitter. The emitter chip was biased from 0 to 3000 V using a source meter (Keithley 2657 A) connected through a resistor of 1 MΩ. The extractor and the collector electrodes were connected to different source meters (Keithley 237) through 100 kΩ and 1 MΩ resistors, respectively. The output voltage to the extractor and collector electrodes was set at 0 V (equivalent to the ground potential) to facilitate the detection of ions colliding against the electrodes.

2.3. Results and discussion

Figure 5 shows the results of ion emission experiments with a single emitter and an array of nine emitters. From the single emitter, ions were extracted at an applied voltage ranging from 2200 to 2300 V, and the maximum extracted ion current was 0.61 μA. From the nine-emitter array, ions were extracted at an applied voltage ranging from 1600 to 2600 V, and only 1.4 μA of ion current was extracted at an applied voltage of 2600 V. Note that electrical short circuits between the emitter and extractor occurred in both cases over the applied voltage shown in the figure. These results indicate that the ion current did not increase in proportion to the number of emitters, which is explained by the large difference in the tip diameters of the nine emitters. The onset voltage of ion emission, V_{start}, can be estimated from the following equation:

$$V_{\mathrm{start}} = \sqrt{\frac{\gamma R_{\mathrm{c}}}{\varepsilon_0}} \ln\left(\frac{4d}{R_{\mathrm{c}}}\right) \tag{1}$$

where γ is the surface tension of the ionic liquid, R_{c} is the curvature radius of the ionic liquid, which has a paraboloidal shape at the emitter tip, ε_0 is the dielectric constant of vacuum, and d

is the distance between the emitters and the extractor electrode.[27] This equation indicates that the onset voltage of ion emission depends significantly on the radius of curvature at the emitter tip. Therefore, emitter tips with different radii of curvature will have different onset voltages, and no ions will be extracted from emitters with relatively large diameter tips. In addition, because the shapes of the tips on the single emitter and nine-emitter array were irregular, the onset voltage and slopes of current–voltage curves were not consistent. We report this initial fabrication process to clarify the design choices we made in a second attempt with a revised approach, which is reported below.

3. Revised fabrication and current measurements

We revised the fabrication process to obtain emitter arrays with uniform emitter tips because the nonuniformity in the emitter tips makes precise control of the extracted ion current difficult, whether the applied voltage or the number of emitters is used to control the ion current.

3.1. Revised fabrication process

Figure 6 shows the revised emitter chip fabrication process. We added two steps to the fabrication process illustrated in Fig. 2. First, the diameter of the resist used as the mask for isotropic etching was adjusted. In the isotropic etching process [Fig. 6(c)], the etching rate increased in proportion to the distance from the center of the emitter array or the wafer. Such a non-uniform etching rate resulted in the non-uniform tip diameters. Therefore, we obtained an isotropic etching rate for each emitter depending on its position, and the mask diameter was

adjusted for each tip so that the resulting tips would be uniform in diameter. Second, we applied a second isotropic etching step [Fig. 6(f)] after removing the resist [Fig. 6(e)]. We found that the etching rates were nearly uniform in the second isotropic etching step. Because the difference in etching rate was caused by local variations in the exposed area,[26] uniform isotropic etching was achieved in the second etching step, for which the exposed area was uniform. Moreover, we reduced the time of the first isotropic etching step that led to the nonuniform etching rate by dividing the isotropic etching process into the two steps shown in Figs. 6(c) and 6(f). The shorter time of the first isotropic etching step minimizes differences in the mask diameter, which allowed us to reduce the differences in the diameters of emitter bases. The second isotropic etching was intended to sharpen the emitter tips without the risk of overetching in the first etching step; overetching often causes the loss of the mask before the anisotropic etching step [Fig. 6(d)], thereby destroying the emitters.

Figure 7(a) shows the photograph of an emitter chip fabricated using the abovementioned revised process. The emitter chip is 18 mm × 18 mm in dimension and encompasses an array of 361 (19 × 19) emitters fabricated within a 13 × 13 mm^2 area in the center of the chip with a pitch of 500 μm. Figure 7(b) shows the emitter at the center of the array, and Figs. 7(c)–7(e) show four emitters at different positions in the array. Figures 8 and 9 show the similarly fabricated emitter chips with 169 (13 × 13) and 81 (9 × 9) emitters, respectively. For the 169- and 81-emitter chips, the pitch of the emitters was 500 μm; the emitters at the outermost row of the emitter array had different base diameters from the rest of

the emitters, depending on the mask diameters. As mentioned earlier, the mask diameters were adjusted in proportion to the etching rate of the first isotropic etching, and the emitter-base diameters were determined by the mask diameter used in the Bosch process. Although the base diameter of some emitters was different, as expected, we successfully obtained uniform and sharp emitter tips, regardless of their positions from the center of the array.

3.2. Experimental setup

The experimental setup for the ion current measurement was almost the same as that described in Sect. 2.2, but the distance between the emitter tip and the extractor was set to d = 0.4 mm to avoid electrical short circuits, and a 70 mm × 70 mm collector electrode was placed at a distance of L = 30 mm from the extractor electrode. In addition, we applied a 1-Hz bipolar pulse voltage to the emitters. For ionic liquid ion sources, an electrochemical double layer is formed between the emitters and the ionic liquid.[28] Because this double layer is very thin, if charge accumulation causes even a small potential difference across the gap between layers, the resulting strong electric field may corrode the emitters and ionic liquid. Charge accumulation across this double layer happens in the order of ~10 s; therefore, a voltage applied at 1-Hz alternating frequency prevents corrosion.[29] Figure 10(a) shows the extractor electrode, which was used for all the arrays (81-, 169-, and 361-emitter chips). The extractor electrode was fabricated from a 525-μm thick silicon wafer using the Bosch process. Figure 10(b) shows a schematic cross-sectional view of the extractor electrode. The 11 mm × 11 mm square groove etched on the wafer surface reduces the thickness of the apertures from 525 to 125 μm. The

diameter of apertures is 300 μm, and the pitch is 500 μm.

We used EMI-DCA as the propellant, and a drop of ionic liquid (0.1 μL) was placed on the reservoir in the same way as in Sect. 2. Figure 11 shows an assembled test device. The emitter chip and the extractor electrode were aligned using microbeads, and they were placed into a polyether ether ketone fixture. As shown in Fig. 11(b), electrical contacts for the emitter and the extractor were connected through the upper fixture holes.

3.3. Results and discussion

Figure 12 shows the results of ion emission experiments with 81-, 169-, and 361-emitter chips. For the 81-emitter chip, the maximum ion current was 22.8 μA on the positive side and the minimum was −19.5 μA on the negative side. For the 169-emitter chip, the maximum ion current was 42.0 μA on the positive side and −36.5 μA on the negative side. For the 361-emitter chip, the maximum ion current was 96.7 μA on the positive side and −87.6 μA on the negative side. These results indicate that the maximum ion current extracted from the emitters increased almost in proportion to the number of emitters, and the maximum ion current was much larger than what we observed previously.[23)]

For all three emitter chips, the slopes of the current–voltage curves decreased at an applied voltage of ~±2400 V. This transition indicates that the current–voltage characteristics changed around these points. The change in voltage dependence around ±2400 V could have arisen from the insufficient flow of ionic liquid to the emitter tips. In a previous study, when high voltage was applied, the emission current from each emitter was limited by the supply of

ionic liquid to emission sites owing to the high hydraulic impedance of the flow paths along the emitter surface.[30] The limited flow rate to the emission sites at high voltages likely explains the transition in the slope of the current–voltage curves.

The current intercepted by the extractor electrode was measured at 1% of the emitter current immediately after the ion emission onset voltage and increased linearly until it reached 15% at the applied voltage of ±2500 V. In the applied voltage range ±(2500–3000) V, the interception fraction was stable at 14%–16%. In addition, no electrical short circuits were observed between the emitter chip and the extractor electrode in any of the emitter chips. These results indicate that the ion emission was stable even when a high voltage was applied. However, a nonnegligible amount of ions was intercepted by the extractor. This rate could be reduced by optimizing the electrode configuration with adjustments to the emitter shapes, extractor aperture diameters, and gap distances. We leave this optimization for future work.

The onset voltage of ion emission was almost equal for all three emitter chips on both the positive and negative sides: 2040 V on the positive side and −2040 V on the negative side for the 81-emitter chip, 2010 V on the positive side and −2010 V on the negative side for the 169-emitter chip, and 2000 V on the positive side and −2010 V on the negative side for the 361-emitter chip; the difference in onset voltage is ≤ 2%. From Eq. (1), one can see that our observation of nearly equal onset voltages at the fixed gap distance d = 0.4 mm implies that differences in the curvature radii of the emitter tips among the three emitter chips were negligible.

Figure 13 plots the ion current per emitter for 81-, 169-, and 361-emitter chips as a function of applied voltage. The current per emitter at ±2400 V was 170 nA on the positive side and −160 nA on the negative side with 361-emitter chip, 168 nA on the positive side and −155 nA on the negative side with 169-emitter chip, and 180 nA on the positive side and −165 nA on the negative side with 81-emitter chip. The differences in these current-per-emitter measurements for three emitter chips at the same applied voltage were small on both the positive and negative sides. Moreover, the slopes of the current–voltage curves on both the positive and negative sides for the different numbers of emitters are similar. This result demonstrates that all the emitters were emitting ions uniformly, which is explained by the uniform-shaped tips forming uniform electric fields around the emitters. These results emphasize that the shape of the emitter tips is a critical factor in ionic liquid electrospray thrusters, and that the ion current can be controlled with the number of emitters or the voltage to the emitters.

4. Conclusions

Toward the development of ionic liquid electrospray thrusters that can be mounted on nano/microsatellites to achieve precise thrust control, we have fabricated and tested needle-emitter arrays from silicon wafers. In preliminary tests, we fabricated single emitter and nine-emitter chips to confirm that ions could be extracted from the emitters. However, the extracted ion current did not increase with the number of emitters because the emitter tips were irregular

in shape, which led to inconsistencies in the current–voltage curves of the emitter chips. To improve the uniformity of the emitter tips, we divided the isotropic etching process into two steps in a revised fabrication process, which was successful.

Ion emission tests showed that the maximum ion current extracted from the revised emitters increased in proportion to the number of emitters on both the positive and negative sides, and emitter chips with various numbers of emitters had almost the same emission onset voltage. This result indicates that all the emitter tips had a uniform radius of curvature. In addition, the ion currents per emitter were same at the same applied voltage and the slopes of the current–voltage curves were similar for all chips with different number of emitters. This result emphasizes that the shape of the emitter tips is critical to the success of such a thruster and further demonstrates that the emitter arrays we fabricated operate uniformly.

In the future work, we plan to measure the ion beam characteristics of emitter arrays fabricated with our process, such as the composition and energy distribution of the ion beam, which we expect to comprise monomers, dimers, trimers, or droplets depending on the conditions.[31,32] Because the mass-to-charge ratio of ions or droplets has a significant effect on the resulting thrust and specific impulse,[33] beam composition will need to be investigated by time-of-flight measurements and the energy distribution will need to be measured using a retarding potential analyzer to estimate thruster performance.[34]

Acknowledgments

This work was supported in part by JSPS KAKENHI (grant number JP18H01623) and JAXA/RDD. A part of this work was conducted at Kyoto University Nano Technology Hub and the Takeda Sentanchi Supercleanroom at The University of Tokyo, supported by the Nanotechnology Platform Program of the Ministry of Education, Culture, Sports, Science and Technology (MEXT), Japan (grant number JPMXP09F-20-UT-0004).

References

1) SpaceWorks, 2020 Nano/Microsatellite Marcket Forecast, 2020.

2) H. Heidt, J. Puig-Suari, A. S. Moore, S. Nakasuka, and R. J. Twiggs, 14th the AIAA/USU Conf. Small Satellites, 2000, SSC00-V-5.

3) D. Lev, R. M. Myers, K. M. Lemmer, J. Kolbeck, H. Koizumi, and K. Polzin, Acta Astronaut. **159**, 213(2019).

4) D. C. Alhorn, J. P. Casas, E. F. Agasid, C. L. Adams, G. Laue, C. Kitts, and S. O'brien, 25th the AIAA/USU Conf. Small Satellites, 2011, SSC11-VI-1.

5) T. Wekerle, J. B. P. Filho, L. E. V. L. Costa, and L. G. Trabasso, J. Aerosp. Technol. Manag. **7**, 269 (2017).

6) T. Toizumi, T. Enomoto, Y. Yatsu, T. Nakamori, N. Kawai, K. Ishizaka, A. Muta, H. Morishita, K. Akiyama, N. Kisa, S. Inagawa, M. Kawakubo, J. Nishida, S. Mizunuma, S. Matsunaga, and J. Kataoka, Physica E **43**, 685 (2011).

7) S. Rucinski, K. Carroll, R. Kuschnig, J. Matthews, and P. Stibrany, Adv. Space Res. **31**, 371 (2003).

8) H. Koizumi, K. Komurasaki, J. Aoyama, and K. Yamaguchi, Trans. Jpn. Soc. Aeronaut. Space. Sci., Aerosp. Technol. Jpn. **12**, Tb_19 (2014).

9) H. Koizumi, H. Kawahara, K. Yaginuma, J. Asakawa, Y. Nakagawa, Y. Nakamura, S. Kojima, T. Matsuguma, R. Funase, J. Nakatsuka, and K. Komurasaki, Trans. Jpn. Soc. Aeronaut. Space. Sci., Aerosp. Technol. Jpn. **14**, Pb_13 (2016).

10) J. Asakawa, H. Koizumi, K. Nishii, N. Takeda, M. Murohara, R. Funase, and K. Komurasaki, Trans. Jpn. Soc. Aeronaut. Space. Sci., Aerosp. Technol. Jpn. **16**, 427 (2018).

11) S. Bandyopadhyay, R. Foust, G. P. Subramanian, S. Chung, and F. Y. Hadaegh, J. Spacecr. Rockets **53**, 567 (2016).

12) G. Bonin, N. Roth, S. Armitage, J. Newman, B. Risi, and R. E. Zee, 29th the AIAA/USU Conf. Small Satellites, 2015, SSC15-I-4.

13) R. Pirayesh, A. Naseri, R. Adcock, S. Stochaj, N. Shah, and J. Krizmanic, 2018 SpaceOps Conference, AIAA Paper-2633.

14) P. Song, L. Sun, S. Kuang, K. Zhang, W. Zou, X. Suo, Y. Wang, D. Xiao, L. Tu, 36th Int. Electric Propulsion Conf., 2019, IEPC-Paper-A-284.

15) M. M. Micci and A. D. Ketsdever, *Micropropulsion for Small Spacecraft* (American Institute of Aeronautics

and Astronautics, Reston, VA, 2000).

16) C. Scharlemann, N. Buldrini, R. Killinger, M. Jentsch, A. Polli, L. Ceruti, L. Serafini, D. DiCara, and D. Nicolini, Acta Astronautica **69**, 822 (2011).

17) G. Taylor, Proc. R. Soc. London, Ser. A **280**, 383 (1964).

18) R. S. Legge and P. C. Lozano, J. Propul. Power **27**, 485 (2011).

19) D. Krejci, F. Mier-Hicks, R. Thomas, T. Haag, and P. Lozano, J. Spacecr. Rockets **54**, 447 (2017).

20) Y. Kitazawa, K. Ueno, and M. Watanabe, Chem. Rec. **18**, 391(2018).

21) F. Mier-Hicks and P. C. Lozano, J. Propul. Power **33**, 456 (2016).

22) D. G. Courtney, H. Shea, K. Dannenmayer, and A. Bulit, J. Spacecr. Rockets **55**, 54 (2018).

23) K. Nakagawa, T. Tsuchiya, and Y. Takao, Jpn. J. Appl. Phys. **56**, 06GN18 (2017).

24) F. Laermer and A. Schilp, U.S. Patent 5 501 893, Mar. 1996.

25) B. Wu, A. Kumar, and S. Pamarth, J. Appl. Phys. **108**, 051101-1 (2010).

26) C. Hedlund, H. O. Blom, and S. Berg, J. Vac. Sci. Technol. A **12**, 1962 (1994).

27) P. Lozano, M. Martínez-Sánchez, and J. M. Lopez-Urdiales, J. Colloid Interface Sci. **276**, 392 (2004).

28) N. Brikner and P. C. Lozano, Appl. Phys. Lett. **101**, 193504 (2012).

29) P. Lozano and M. Martínez-Sánchez, J. Colloid Interface Sci. **280**, 149 (2004).

30) F. A. Hill, E. V. Heubel, P. P. De Leon, and L. F. Velasquez-Garcia, J. Microelectromechanical Syst. **23**, 1237 (2014).

31) S. Dandavino, C. Ataman, C. N. Ryan, S. Chakraborty, D. Courtney, J. P. W. Stark, and H. Shea, J. Micromech. Microeng. **24**, 075011 (2014).

32) D. G. Courtney and P. Lozano, Trans. Jpn. Soc. Aeronaut. Space Sci., Aerosp. Technol. Jpn. **8**, Pb_73 (2010).

33) D. M. Goebel and I. Katz, *Fundamentals of Electric Propulsion: Ion and Hall Thrusters* (Wiley, Hoboken, NJ, 2008).

34) P. C. Lozano, J. Phys. D: Appl. Phys. **39**, 126 (2006).

List of Figure Captions

Fig. 1. Schematic of the externally-wetted electrospray thruster. High positive/negative voltage is applied to the emitter while the extractor electrode is grounded.

Fig. 2. Steps in the fabrication of small emitter arrays for preliminary tests. (a) First, a silicon wafer coated with a thick positive-type photoresist (PMER P-LA900PM) is exposed and developed. (b) Second, isotropic etching using SF_6 is performed to form the cone shape of the emitter tips. (c) After that, anisotropic etching using the Bosch process is performed to form the cylindrical shape of the emitters. (d) Finally, the photoresist is removed.

Fig. 3. (a) Image of a fabricated emitter chip with a single emitter. (b) SEM images of the single emitter and (c) the emitter tip. (d) Image of a fabricated emitter chip with nine emitters. (e) SEM images of the emitter at the center of the nine emitters and (f) the emitter on the far left of the nine emitters, 2.0 mm away from the center of the array.

Fig. 4. (a) Schematic of the experimental setup for the ion current measurements, where *d* and *L* are the gab distance between the emitter and extractor and the distance between the extractor and collector, respectively. Photographs of the extractor electrodes made of 0.08-mm thick stainless steel for (b) the single emitter and (c) the nine-emitter array.

Fig. 5. Collector current (solid circles), extractor current (open squares), and emitter current (solid triangles) as functions of applied voltage for (a) the single emitter and (b) the nine-emitter array.

Fig. 6. Modified process for fabricating the emitter arrays. (a) Silicon wafer coated with a thick positive-type photoresist (AZ P4620) is exposed by a laser direct writing and (b) developed, where the diameters of the resist for each emitter are adjusted according to the isotropic etching rate. (c) Isotropic etching using SF_6 and (d) anisotropic etching using the Bosch process are performed. (e) The resist is removed from the emitter tips. (f) Isotropic etching is repeated to form sharp emitter tips.

Fig. 7. (a) Image of a fabricated chip with 361 emitters. (b) SEM images of the center of the array, and of four emitters at distances of (c) 2.12 mm, (d) 3.54 mm, and (e) 5.66 mm from the center of the array.

Fig. 8. (a) Image of a fabricated chip with 169 emitters. (b) SEM images of the emitter at the center of the array, and emitters at distances of (c) 0.71 mm, (d) 2.12 mm, and (e) 3.54 mm from the center of the array.

Fig. 9. (a) Image of a fabricated chip with 81-emitter chip. (b) SEM images of the emitter at the center of the array, and emitters at distances of (c) 1.41 mm, (d) 2.82 mm, and (e) 5.66 mm from the center of the array.

Fig. 10. (a) Image of an extractor electrode fabricated from a 525-μm thick silicon wafer. (b) Schematic cross-sectional view of the extractor electrode taken along the white dotted line in Fig. 10(a).

Fig. 11. Image of (a) the aligned emitter chip and the extractor electrode, and (b) the assembled device.

Fig. 12. Collector current (solid circles), extractor current (open squares), and emitter current (solid triangles) of (a) 81-emitter chip, (b) 169-emitter chip, and (c) 361-emitter chip as functions of the applied voltage.

Fig. 13. Current per emitter for 361-(solid circles), 169-(solid triangles), and 81-(open squares) emitter chips as functions of the applied voltage.

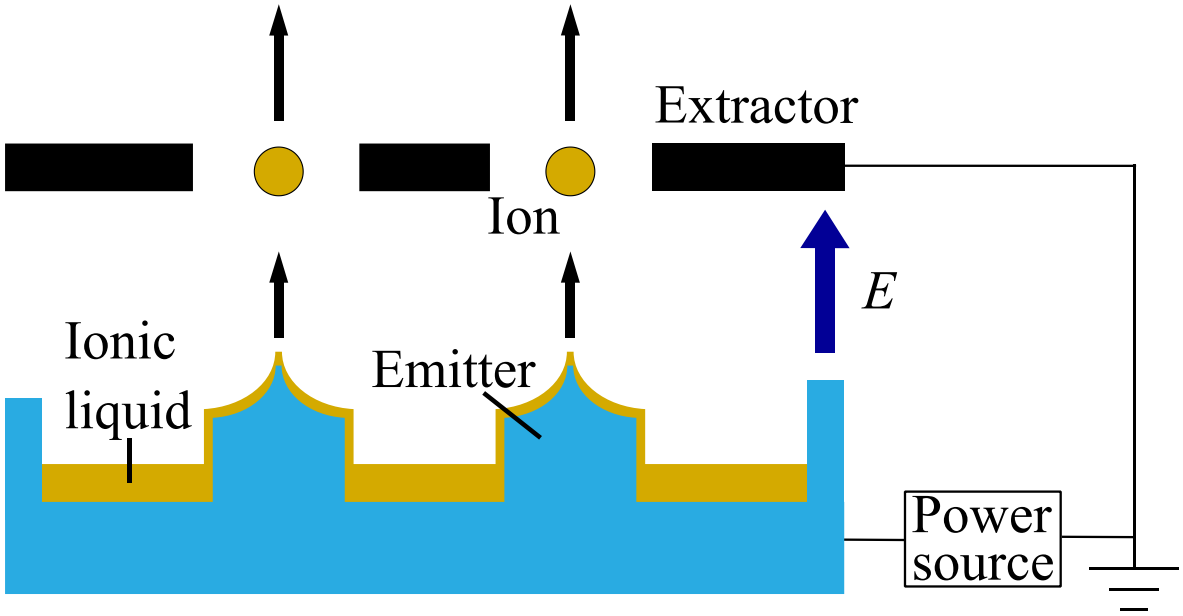

Fig. 1

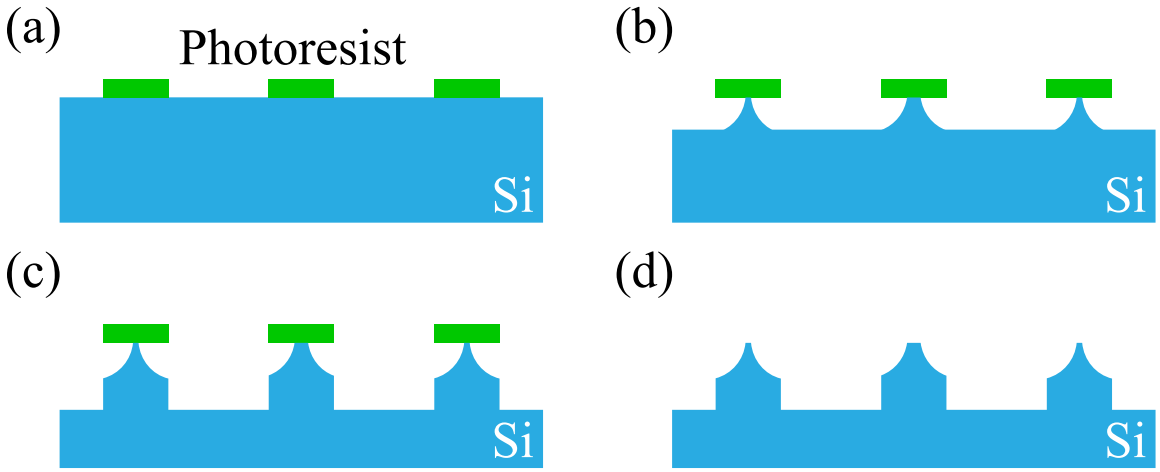

Fig. 2

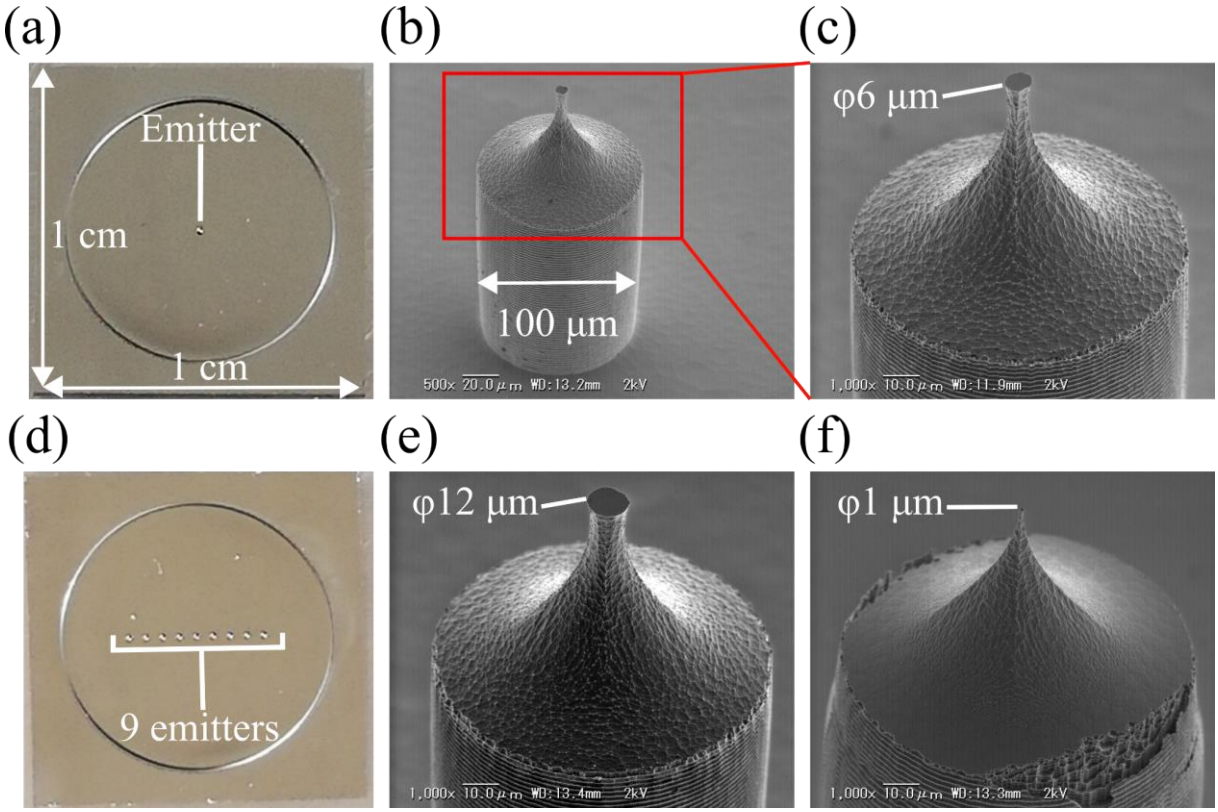

Fig. 3

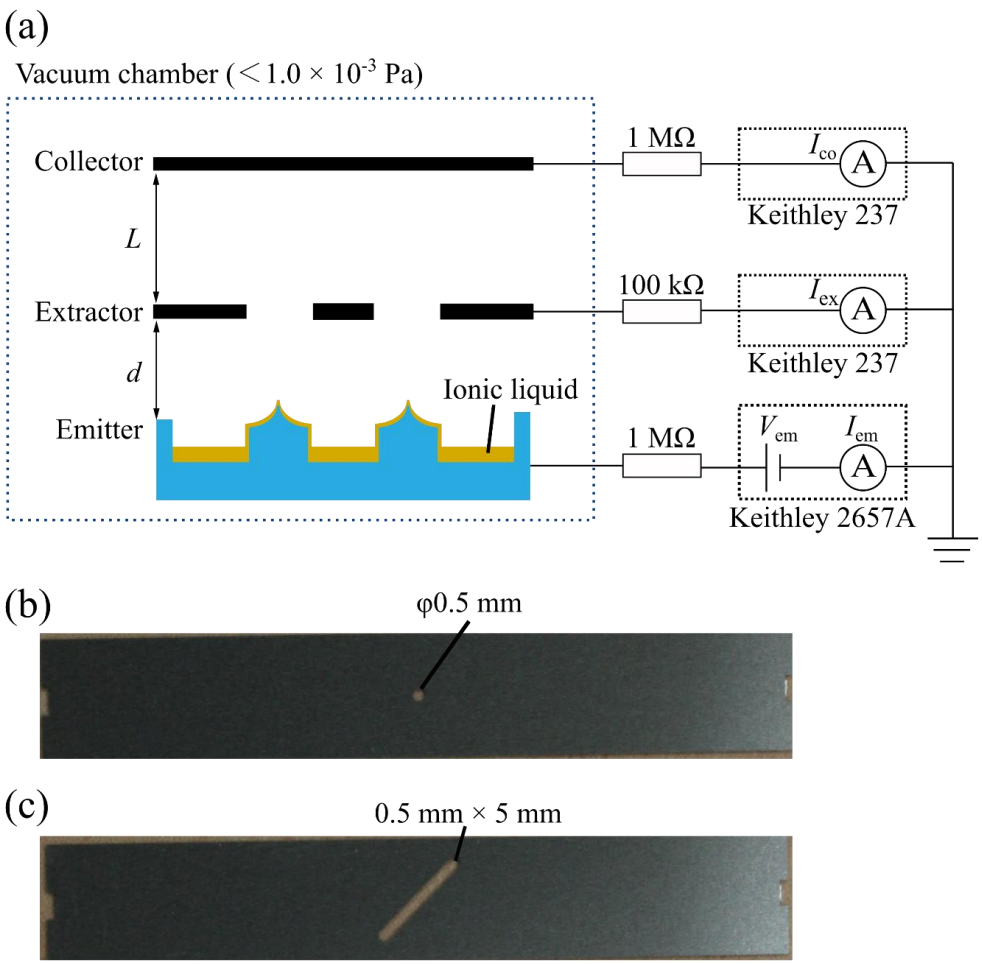
(a)
Vacuum chamber (< 1.0 × 10-3 Pa)
Collector
L
Extractor
d
Emitter
Ionic liquid
1 MΩ
Ico
A
Keithley 237
100 kΩ
Iex
A
Keithley 237
1 MΩ
Vem
Iem
A
Keithley 2657A
(b)
φ0.5 mm
(c)
0.5 mm × 5 mm

Fig. 4

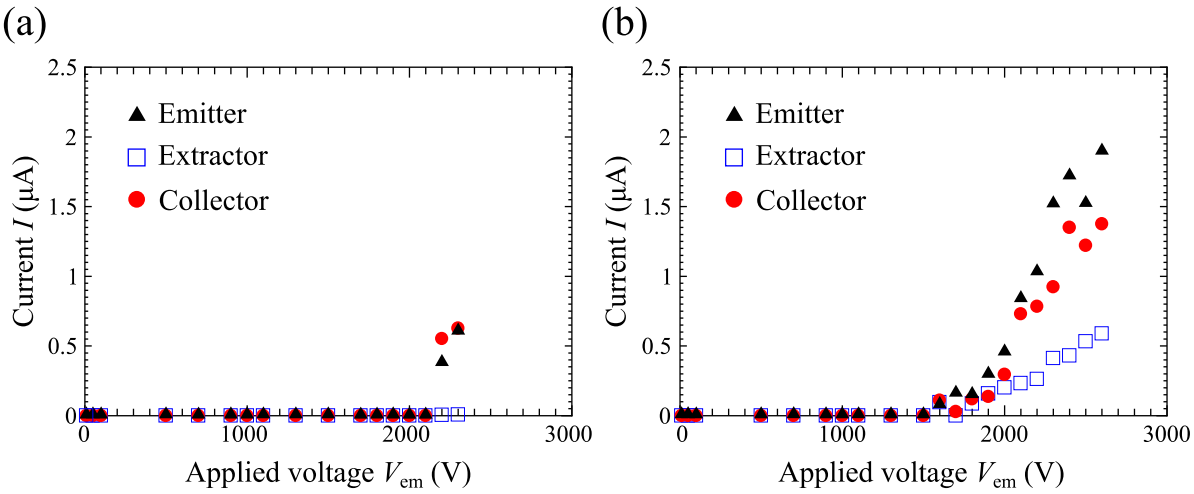
(a)
(b)
Emitter
Extractor
Collector
Current I (μA)
Applied voltage V_{em} (V)
0
0.5
1
1.5
2
2.5
1000
2000
3000

Fig. 5

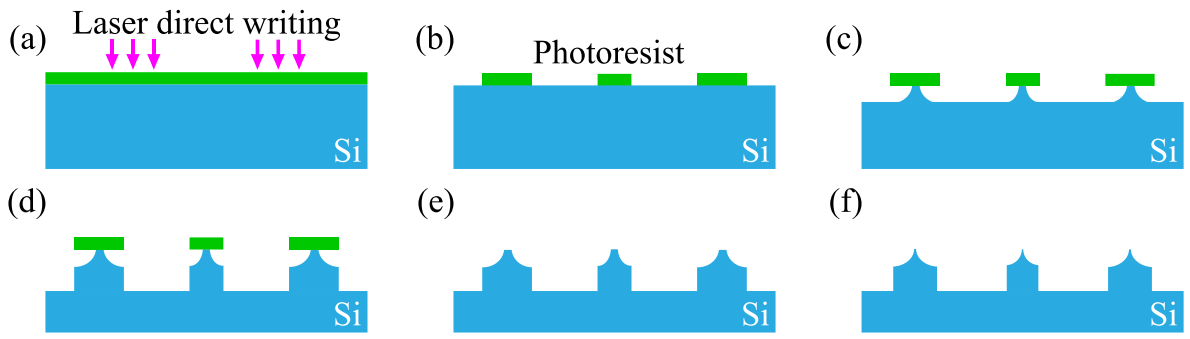

Fig. 6

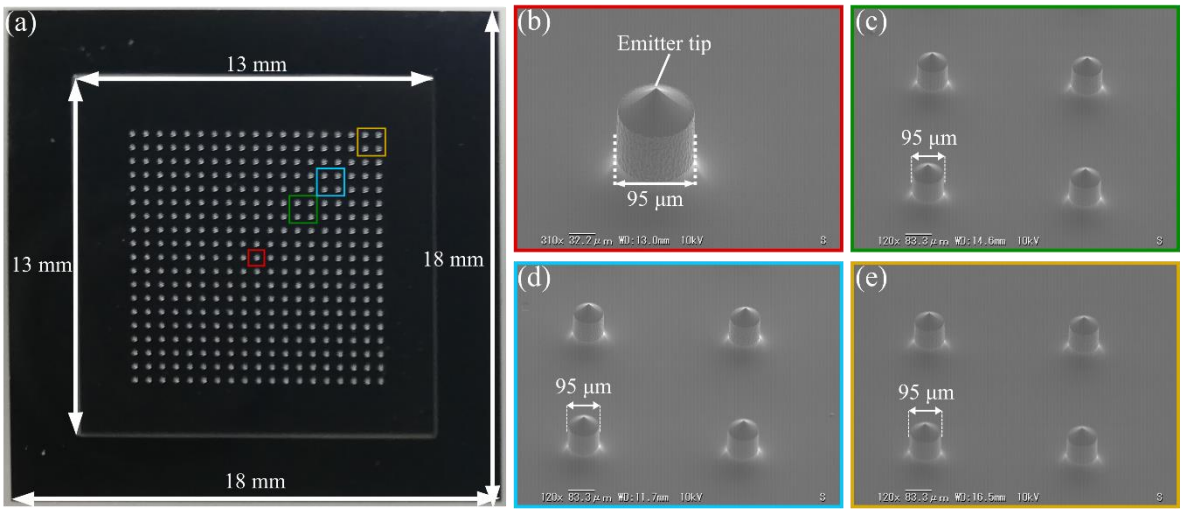

Fig. 7

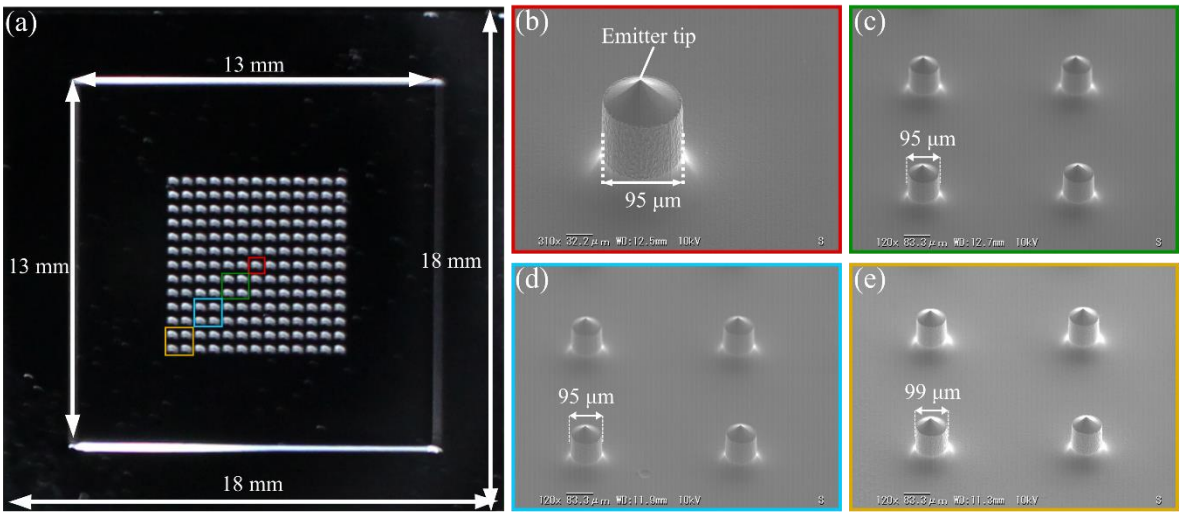

Fig. 8

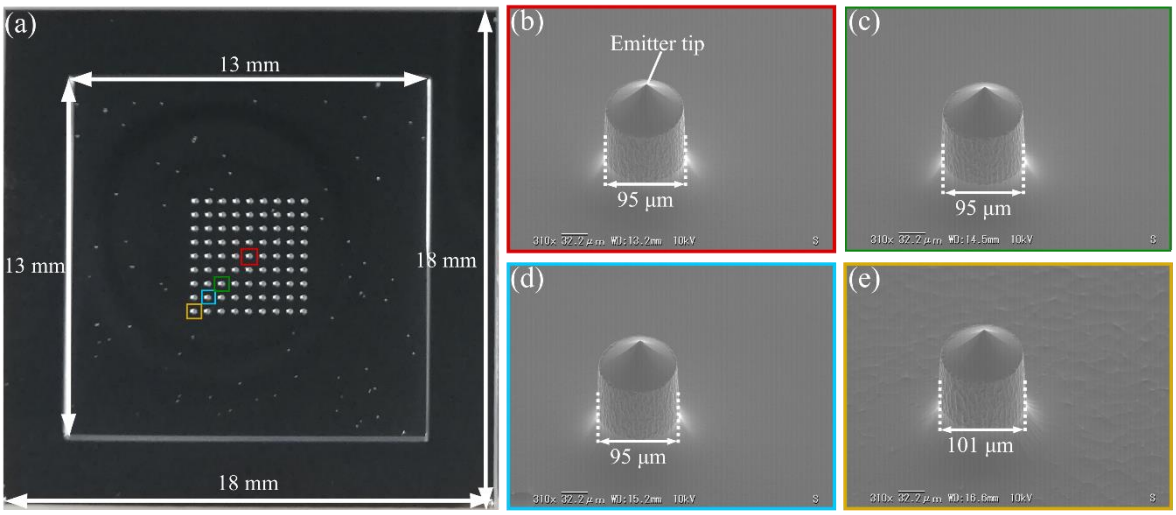

Fig. 9

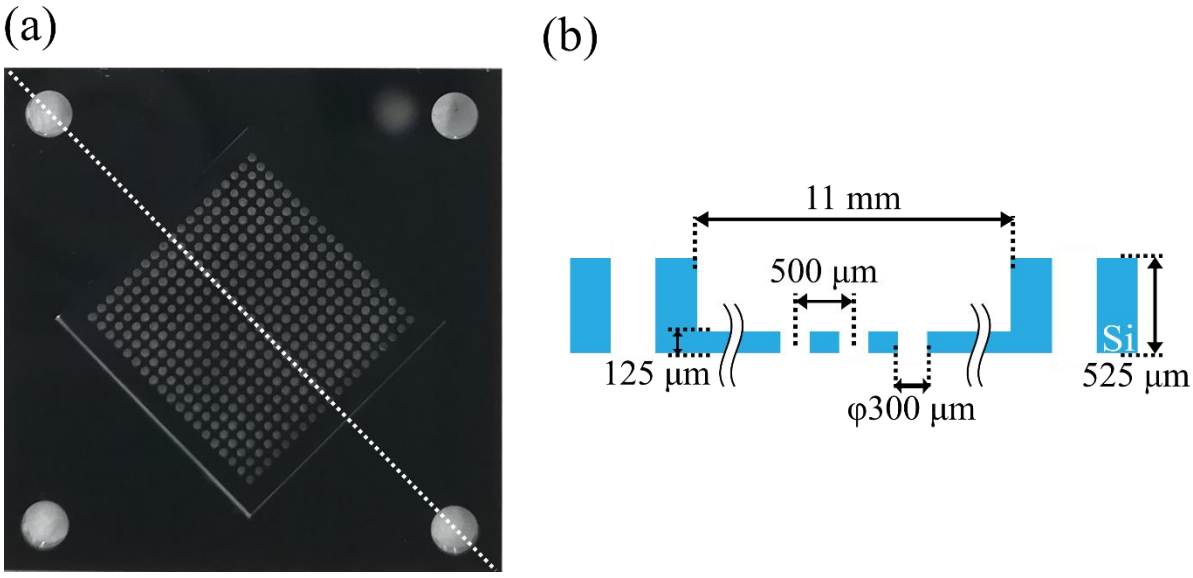

Fig. 10

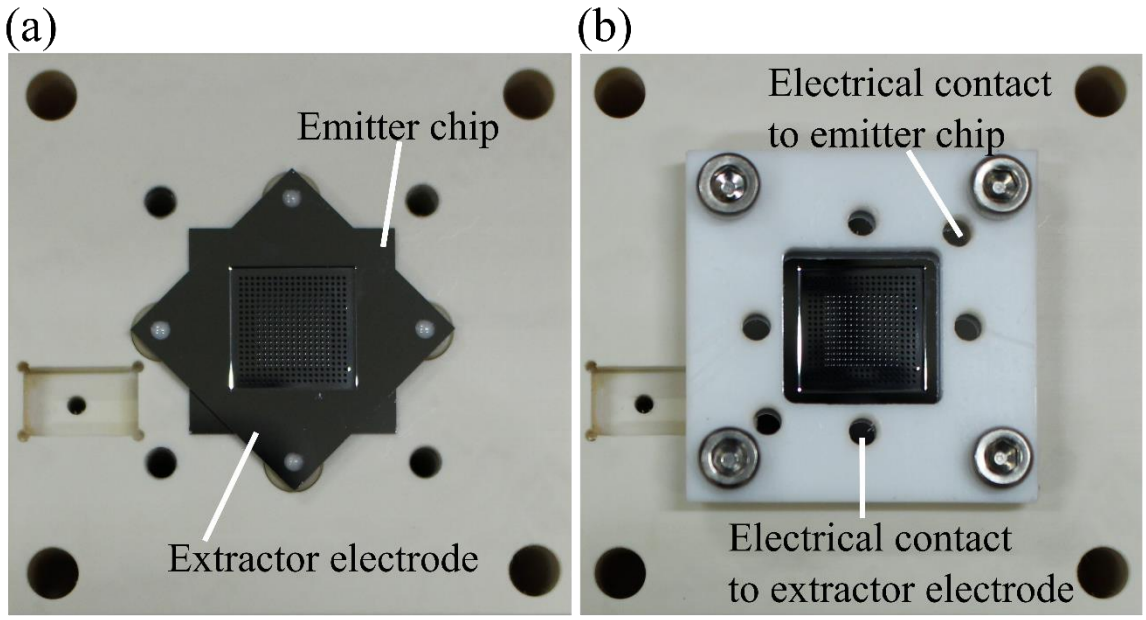
(a)
Emitter chip
Extractor electrode
(b)
Electrical contact
to emitter chip
Electrical contact
to extractor electrode

Fig. 11

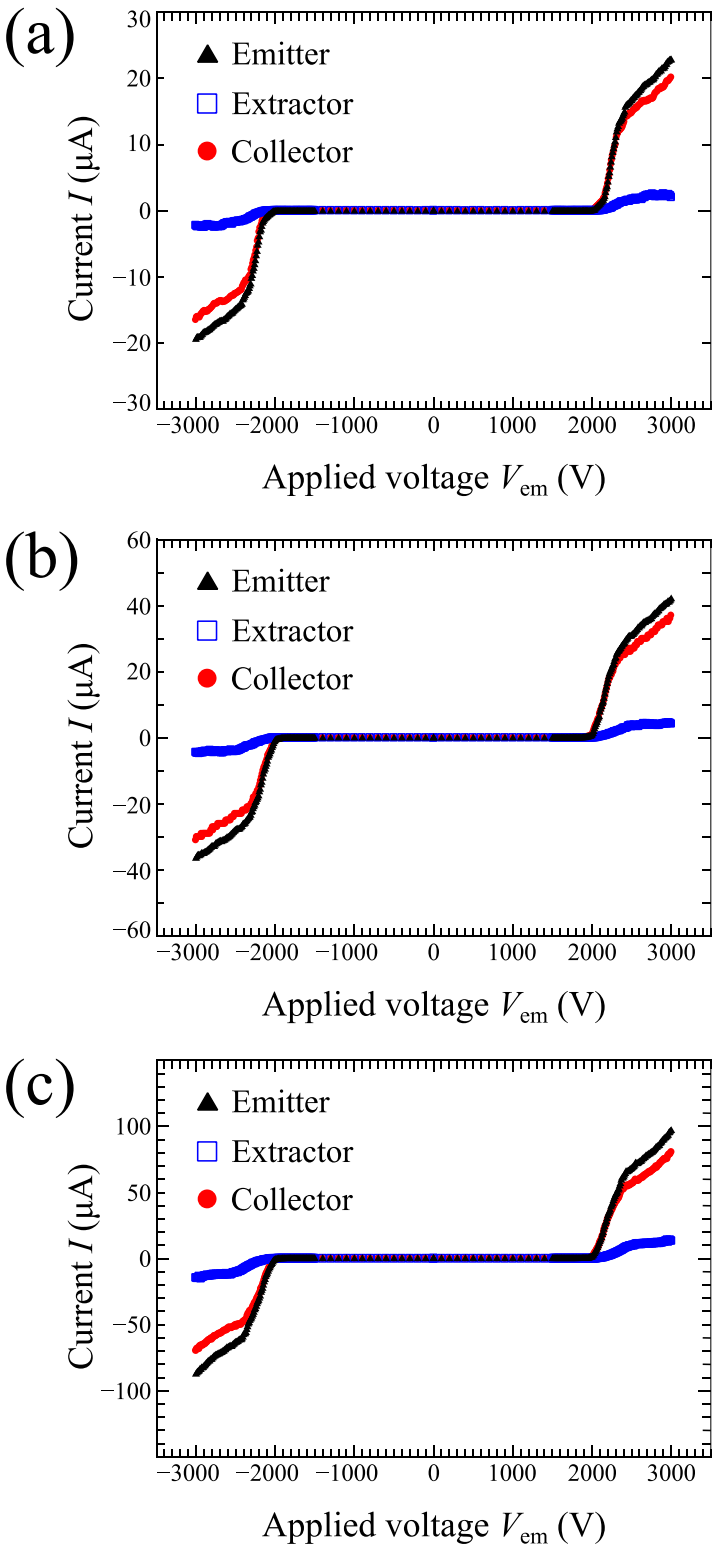
(a)
Emitter
Extractor
Collector
Current I (μA)
Applied voltage V_em (V)
(b)
Emitter
Extractor
Collector
Current I (μA)
Applied voltage V_em (V)
(c)
Emitter
Extractor
Collector
Current I (μA)
Applied voltage V_em (V)

Fig. 12

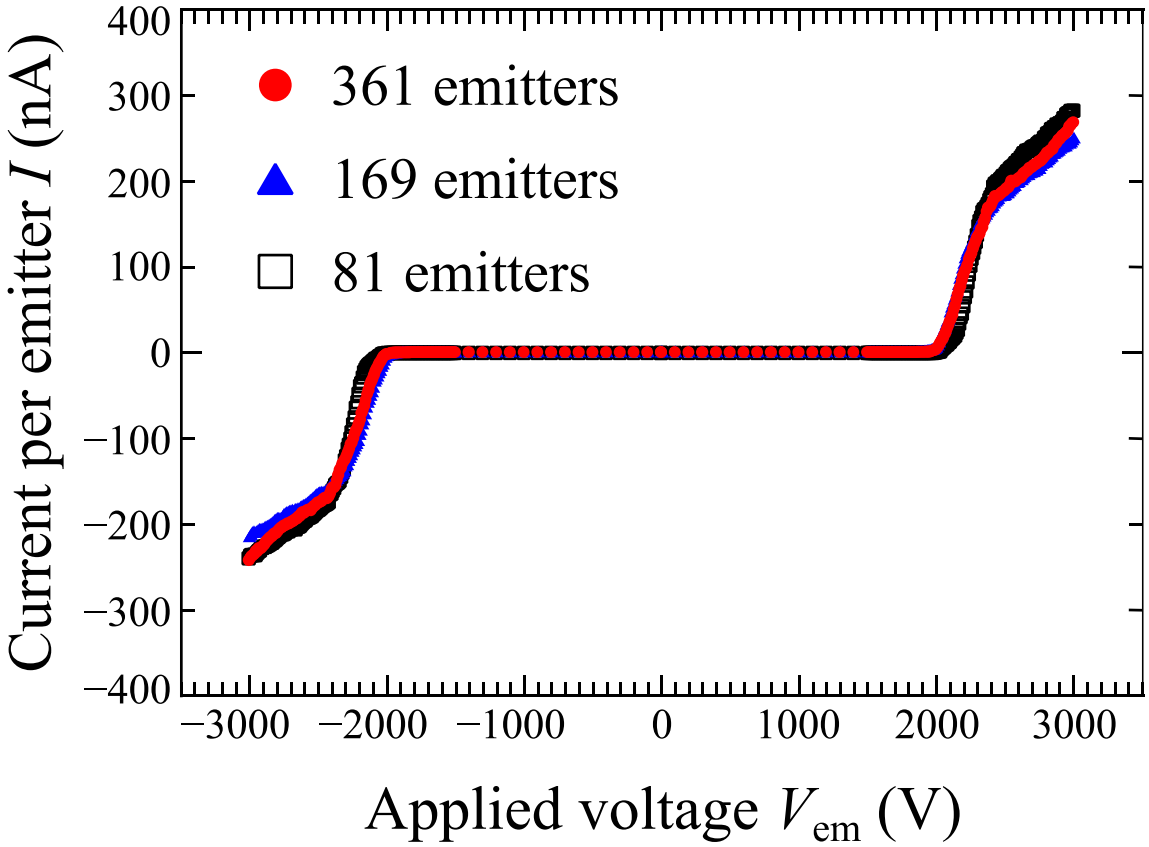
400
300
200
100
0
−100
−200
−300
−400
Current per emitter I (nA)
361 emitters
169 emitters
81 emitters
−3000
−2000
−1000
0
1000
2000
3000
Applied voltage V_{em} (V)

Fig. 13